JOURNAL OF Materials CHEMISTRY

The hydroxylation of t-ZrO_2 surfaces

Susan E. Redfern,[a] Robin W. Grimes*[a,b] and Rees D. Rawlings[a]

[a]*Dept. Materials, Imperial College of Science, Technology and Medicine, Prince Consort Road, London, UK SW7 2BP. E-mail: r.grimes@ic.ac.uk*
[b]*Los Alamos National Laboratory, PO Box 1663, MS K765, Los Alamos NM 87545, USA*

Received 26th September 2000, Accepted 26th October 2000
First published as an Advance Article on the web 5th January 2001

Atomistic simulation techniques have been used to model the dissociative adsorption of water onto the (100), (101) and (110) surfaces of tetragonal zirconia. A number of partial coverages up to a full monolayer have been investigated. Results show that hydroxylation energies depend greatly on the surface in question, although a general trend of decreasing hydroxylation energy with increasing coverage is observed on all surfaces studied. In the case of the (101) surface, hydroxylation energies are positive at all coverages investigated, indicating that a layer of dissociated water will not form, while the hydroxylation energies of the (100) and (110) faces predict that a 50% monolayer will form.

1 Introduction

Zirconia exists in three allotropic forms.[1] The high temperature form is cubic (c), which transforms to the tetragonal phase (t) at 2370 °C; the latter is stable until around 1000 °C at which point the monoclinic phase (m) is formed. Phase stability and transformation, particularly the t→m transformation, in pure and doped zirconia have been studied by a variety of techniques, both experimental[2–4] and theoretical.[5–8]

The t→m transformation is accompanied by a large volume expansion of about 3%. A consequence of the volume expansion is that polycrystalline samples of pure zirconia fracture when cooled from the fabrication (sintering) temperature to room temperature. For this reason, components are not manufactured from polycrystalline pure zirconia. The problem is overcome by the addition of controlled amounts of oxides, known as stabilising oxides, that suppress the t→m transformation to varying extents. For example, 8 mol% yttria addition fully stabilises the cubic phase at room temperature. Ceramics with this amount of yttria addition are known as cubic stabilised zirconia (CSZ) and are employed as the electrolyte in solid oxide fuel cells.[9] On the other hand, 3 mol% yttria, together with a small grain size, results in a ceramic with a metastable tetragonal structure at room temperature; these are referred to as tetragonal zirconia polycrystalline (TZP) ceramics. The ceramic remains in the tetragonal state at room temperature because of the presence of the stabilising oxide and the elastic constraint of the neighbouring grains hindering the expansion. The elastic constraint increases with decreasing grain size, hence the need for a small grain size.

TZPs have outstanding mechanical properties that are the result of the t→m transformation occurring by a displacive, diffusionless transformation at the crack tip.[1,10] The transformation occurs because the crack tip stresses relax the elastic constraint. The volume expansion associated with the small amount of material that has transformed induces compressive stresses on the crack faces, which hinder crack propagation. A structural application of TZP is as the femoral head in a hip prosthesis.[11]

Unfortunately, TZPs are sensitive to moisture at moderate (>60 °C) temperatures.[12–21] Moisture causes the t→m transformation to take place in an uncontrolled manner at the surface and this is accompanied by a degradation of mechanical performance.[e.g. 12–13] Several mechanisms for the process have been proposed, such as preferential dissolution of yttria,[14] annihilation of oxygen vacancies[15] and a decrease in the difference between the surface energies of the tetragonal and monoclinic phases.[16] Recent investigations[17–19] have been concentrated at the microstructural level and have demonstrated that the transformation is nucleated, apparently at a constant rate, and that the transformed regions grow at a constant rate. Little is known about the nucleation stage, *i.e.* why does moisture cause a given region to transform and nucleate the reaction in preference to another region? Small variations in composition and/or grain size may lead to the transformation of low stabilising oxide content regions and/or large grains. Another possibility is that the affinity of water vapour for a surface depends on the crystallography of the surface: this is investigated in the current paper.

We have used atomistic simulation techniques to carry out an investigation into the effect of water adsorption onto tetragonal zirconia surfaces. We are particularly interested in the energies of hydroxylation of the different faces, to determine if the degree of hydroxylation is orientation dependent.

Using atomistic simulation techniques, we have modelled the (100), (101) and (110) faces of tetragonal zirconia under vacuum conditions and after the formation of a hydroxy layer. Partial monolayer coverages of 25, 50, 75 and 100% have been investigated. The surface structures and energetics are discussed, and the changes in relative surface energies on hydroxylation are illustrated by calculating the equilibrium crystal morphologies under wet and dry conditions.

2 Theoretical methods

Interactions between lattice ions are based on the Born model of solids.[22] The major contribution to the lattice energy is derived from the long-range Coulombic interactions, which for surfaces are summed using Parry's modification of Ewald's method[23–25] to ensure convergence. Short-range attractions and repulsions are described using parameterised pair-potentials. The polarisability of the ions must also be taken into account and is described using the shell model.[26] This consists of a core with charge $Y|e|$ and a massless shell with charge $X|e|$, connected *via* a spring with spring constant κ. The values of Y and κ are given in Table 1.

The potential model used to describe the interactions between the oxygen and hydrogen atoms of the hydroxyl

Table 1 Potential Parameters used in this work

	Buckingham potentials (short range cut-off 20 Å)		
Ion pair	A/eV	ρ/Å	C/eV Å^6
O^{2-}–O^{2-}	9547.96	0.224	32.0
O^{2-}–Zr^{4+}	1502.11	0.345	5.1
O^{2-}–$H^{0.4+}$	591.35	0.2114	0.0
$O^{1.4-}$–$O^{1.4-}$	11278.54	0.207218	16.0
$O^{1.4-}$–$H^{0.4+}$	4220.76	0.103234	0.0
$O^{1.4-}$–Zr^{4+}	1450.94	0.32689	0.0
$O^{1.4-}$–O^{2-}	10364.15	0.2373	22.63
	Dampened Coulomb potentials (short range cut-off 20 Å)		
$O^{1.4-}_{core}$–$H^{0.4+}$	—	0.479177	—
$O^{1.4-}_{shell}$–$H^{0.4+}$	—	0.479177	—
	Core–shell interactions		
Ion	κ/eV Å^{-2}	Y	
O^{2-}	6.3	−2.04	
$O^{1.4-}$	75.57	−2.30	
Zr^{4+}	253.3	−0.05	

groups must take into account the strong degree of overlap between these species due to the short inter-atomic separation of approximately 1 Å. Consequently, we have developed a 'dampened Coulombic potential' where the electrostatic interaction between ions O and H decreases exponentially as the ionic separation, r_{OH}, is decreased. The form of the potential is:

$$V(r_{OH}) = \left(\frac{q_O q_H}{4\pi\varepsilon_o r_{OH}}\left(1 - \exp\left(\frac{-r_{OH}}{\rho}\right)\right)\right) \quad (1)$$

Since we employ a shell model[26] for oxygen, the damping term in eqn. 1 acts between the oxygen shell and hydrogen and the oxygen core and hydrogen (see parameters in Table 1). This Coulomb potential model is used in conjunction with a Buckingham potential to describe short-range repulsive forces

$$E(r_{ij}) = Ae^{-r_{ij}/\rho} - C/r_{ij}^6 \quad (2)$$

where r_{ij} is the separation between ions i and j; A, ρ and C are adjustable parameters. Since the Coulomb damping term has negligible effect at non-bonded O–H separations, the interaction between non-bonded oxygen and hydrogen is the same as in conventional potential models.[27,28] Although our model for bonded O–H is different to the usual Coulomb subtracted Morse potential,[27,28] it has two advantages. First, it is not necessary to specify ranges within which the two different models act and second, the potential has continuous derivatives. The disadvantage is that the parameters in the present model do not correspond to measured values such as dissociation energy and O–H bond distance, as they do with the Morse potential model.

The cation–oxygen and oxygen–oxygen short-range interactions are described by Buckingham potentials. These were fitted empirically so that they satisfactorily reproduced experimental lattice parameters and atomic positions of a range of compounds (see Table 1). For example, the Zr^{4+}–O^{2-} parameters were fitted to the structures of both cubic and tetragonal zirconia,[29,30] and the parameters used to describe the hydroxy group were fitted to the crystal structures of $Ca(OH)_2$, $Mg(OH)_2$ $Fe(OH)_2$, NaOH, $Y(OH)_3$, FeOOH and AlOOH.

Unfortunately, no crystal structure data could be found to which the interaction between the Zr^{4+} cation and the oxygen of the hydroxide group ($O^{1.4-}$) could be fitted. This potential model was therefore obtained by assuming that the difference between the two previously fitted potentials of Y^{3+}–$O^{1.4-}$ and Y^{3+}–O^{2-} is equal to that between Zr^{4+}–$O^{1.4-}$ and Zr^{4+}–O^{2-}. Since the former has already been established *via* fitting to $Y(OH)_3$ and Y_2O_3, the Zr^{4+}–$O^{1.4-}$ potential can thereby be deduced. The potential models used in this work are given in Table 1.

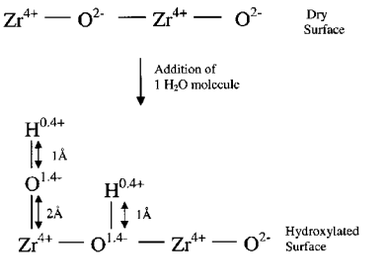

Fig. 1 Schematic representation of the creation of the initial hydroxylated surface configuration.

2.1 Calculation of surface energy

The surface structures were calculated using the code MARVINS.[31] In this code, the surface energy of a perfect surface, γ, is defined as the excess energy of the surface ions compared to the same number of bulk ions, and is expressed per unit area *i.e.*

$$\gamma = \frac{U_{surf} - U_{bulk}}{\text{Area}} \quad (3)$$

The hydroxylated surfaces were initiated by positioning an (OH) group directly above a surface cation (at a Zr–O distance of 2 Å) with the hydrogen atom above the oxygen atom (see Fig. 1). A surface oxygen was also protonated (the hydrogen atom being placed 1 Å above the oxygen), completing the addition of one water molecule. This was repeated until the required coverage was reached. The surface was then allowed to relax *via* energy minimisation. A full (100%) monolayer is defined as 1 water molecule per surface cation or oxygen atom.

The energy of hydroxylation is calculated *via* the energy cycle shown in Fig. 2. If the energy values of all the individual steps are summed, the total is equal to the energy of hydroxylation per 2 water molecules adsorbed. The first and final steps are the surface block energies of the dry and hydroxylated surfaces respectively, and as such are dependent on the surface in question. The intermediate steps depend only on the properties of zirconia and therefore can be transferred between all calculations. Step (a) is the sum of the first and second electron

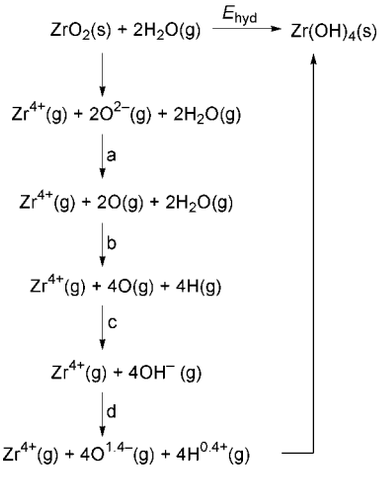

Fig. 2 Born–Haber cycle used in the calculation of hydroxylation energies, E_{hyd}.

affinities of oxygen in zirconia. The second electron affinity of oxygen on ZrO_2 is calculated *via* the Born–Haber cycle in Fig. 3. The values used are given in Table 2. This gives a value for the second electron affinity of oxygen in ZrO_2 of 7.52 eV. The total energy of steps (a)–(d) in Fig. 2, E_{corr}, is 9.6 eV, *i.e.* 4.8 eV per water molecule adsorbed.

The energy of hydroxylation and hydroxylated surface energy with respect to gaseous water can then be calculated using the following formulae:

$$E_{hyd} = \left[\frac{(U_{surf}(hyd) - U_{surf}(dry))}{n}\right] + E_{corr} \quad (4)$$

where U_{surf} is the total energy of the surface block and n is the number of adsorbed water molecules. The surface energy of the hydroxylated surface γ, is then given by:

$$\gamma_{hyd} = \frac{[(U_{surf}(hyd) - U_{bulk}) + (nE_{corr})]}{Area} \quad (5)$$

The effect of water adsorption on the surface structure and energetics is described in detail in section 3.

3 Results

The simulation model correctly reproduces the space group of tetragonal zirconia, $P4_2/nmc$. Furthermore, the calculated structural parameters are in good agreement with experiment as shown in Table 3, giving us confidence in the accuracy of the potential model.

In the following sections, the atomic scale structure of the relaxed dry and hydroxylated surfaces will be discussed. Hydroxy groups formed by the protonation of a surface oxygen atom will be denoted type α, whilst those formed above surface cations will be designated as type β. All partial coverages investigated are discussed, including brief sections on those not predicted to occur by energetics, as these are useful in understanding why the monolayer is not completed. The energies of hydroxylation and hydroxylated surface energies are given in Table 4.

3.1 The (100) surface

3.1.1 Dry (100) surface. This surface is a type I surface[37] *i.e.* each layer contains stoichiometric amounts of ZrO_2. The surface layer contains 6-fold Zr ions and 3-fold O ions, compared to their bulk crystal co-ordinations of 8- and 4-fold respectively. Under vacuum conditions, this surface undergoes minimal relaxation. The Zr ions in the uppermost layer move towards the bulk by 0.23 Å and the O ions in the same layer move 0.07 Å in the same direction. In the second layer, the oxygen ions move approximately 0.1 Å from their equilibrium positions, but the Zr cations move 0.14 Å towards the surface. All other ions in the crystal *i.e.* those more than 4 Å from the surface relax 0.05 Å or less from their bulk positions (see Fig. 4(a)).

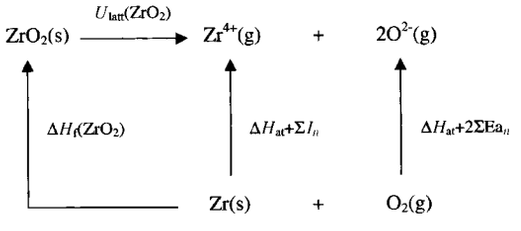

Fig. 3 Born–Haber cycle for the formation of ZrO_2. U_{latt} is the lattice energy, ΔH_f is the enthalpy of formation, ΔH_{at} is the enthalpy of atomisation of the cation, ΔH_{diss} is the enthalpy of dissociation of diatomic oxygen, I_n is the n^{th} ionisation energy of the cation and Ea_n is the n^{th} electron affinity of oxygen.

Table 2 Component energies for the Born–Haber cycle, where ΔH_f is the enthalpy of formation, ΔH_{diss} is the enthalpy of dissociation, I_n is the n^{th} ionisation energy of the cation and Ea_n is the n^{th} electron affinity of the anion

Reaction	Value/eV
ΔH_f ZrO_2(s)	−11.41[32]
ΔH_f (H_2O(g))	−2.51[32]
ΔH_f (H(g))	+2.26[32]
ΔH_f (O(g))	+2.58[32]
ΔH_f (OH(g))	+0.40[32]
ΔH_f (OH^-(g))	−1.46[32]
ΔH_f (Zr(g))	+6.31[33]
I_1 (Zr)	+6.63[34]
I_2 (Zr)	+13.13[34]
I_3 (Zr)	+22.99[34]
I_4(Zr)	+34.34[34]
ΔH_{diss} (O_2)	+5.12[35]
Ea_1 (O)	−1.47[36]

Table 3 Calculated and experimental lattice parameters of tetragonal zirconia

	Lattice parameters		Atomic position of oxygen in asymmetric unit cell		
	a	*c*	*x*	*y*	*z*
Experimental	3.5935	5.189	0.0	0.5	0.185
Calculated	3.5924	5.123	0.0	0.5	0.218

3.1.2 25% Coverage. The effect of surface relaxation on the ZrO_2 crystal in the presence of water is such that Zr ions further than 5 Å below the surface are less than 0.05 Å from their equilibrium positions, but displacements of oxygen ions of more than 0.1 Å are found up to 9 Å from the surface, *i.e.* the presence of a hydroxy layer increases the relaxation of the crystal. Additionally, shifts in the positions of the (OH) groups are much greater than those of Zr or O in the lattice. For example, oxygen ions now part of type α (OH) groups move out of the relaxed surface plane by 1.5 Å to be almost in plane with the type β groups with which they interact *via* the hydrogen atom to the oxygen atom at a $(OH)_{non\text{-}bonded}$ distance of 2.15 Å. For comparison, the hydrogen bonding separation found in ice is between 1.76 and 1.95 Å.[38]

Both types of hydroxy group tilt towards the surface on relaxation, type α to a greater extent (30° compared to approximately 70° for type β). The bond length within the hydroxy groups is found to depend on the distance from the surface. Those closer to the surface, type α, have a bond length of 0.96 Å whereas type β groups, further from the surface, have a shorter bond length of 0.91 Å. The hydroxylation energy released at this coverage is over 1 eV per water molecule adsorbed (see Table 4), indicating a strong driving force to form a hydroxy layer.

3.1.3 50% Coverage. In this case, the relaxation of the ZrO_2 crystal is greater than at 25% coverage. Only 1 in 25 of the O ions in the first 6 layers change position by over 0.3 Å at 25% coverage, but this now rises to almost 1 in 7. The arrangement of hydroxy groups is also different (Fig. 5(a)). Type β hydroxy groups are more upright than at 25% coverage, and positioned 2 Å above the relaxed surface plane (O–H distance 0.90 Å), while type α (OH) groups lie flat, parallel to the relaxed surface plane, but approximately 1 Å above it (O–H distance 0.92 Å). An interaction between the H atom and a surface oxygen atom leads to an $(OH)_{non\text{-}bonded}$ distance of 2.15 Å, the same separation as between the two types of hydroxy group at 25% coverage.

Table 4 Hydroxylation energies (per water molecule adsorbed), E_{hyd} and hydroxylated surface energies, γ_{hyd}

	Partial monolayer coverage								
		25%		50%		75%		100%	
Surface	Dry γ/J m^{-2}	E_{hyd}/eV	γ/J m^{-2}	E_{hyd}/eV	γ/J m^{-2}	E_{hyd}/eV	γ/J m^{-2}	E_{hyd}/eV	γ/J m^{-2}
(100)	2.57	−1.22	2.30	−1.09	2.09	−0.50	2.23	−0.10	2.48
(101)	1.65	+0.98	2.00	+0.78	2.20	+1.29	3.03	+1.56	3.86
(110)A	2.65	−0.42	2.52	−0.32	2.45	−0.15	2.51	−0.02	2.62
(110)B	2.63	−1.27	2.24	−0.71	2.19	−0.16	2.48	−0.01	2.62
(110)C	4.10	−3.05	3.63	−4.50	2.72	−2.89	2.77	−2.06	2.84

The hydroxylation energy per water molecule of the (100) surface at 50% coverage is less than at 25% (see Table 4). However, the reduction of the (100) surface energy due to a 50% coverage is greater than due to 25% coverage and therefore a 50% coverage is predicted if sufficient water is available. In fact, this is the highest density water layer we predict will form on this face.

3.1.4 75 and 100% Coverage. At 75% coverage, the surface relaxation of the ZrO_2 crystal is very similar to that at 25% coverage. Type β (OH) groups remain approximately 2 Å above the surface, although not directly above Zr cations. Type α groups move to positions up to 0.9 Å above the relaxed plane. Interactions between the two types of group lead to $(O–H)_{non\text{-}bonded}$ separations as low as 1.5 Å, shorter than at the lower coverages.

At full (100%) monolayer coverage the relaxation of the ZrO_2 crystal is reduced. Both types of hydroxy group are arranged in rows along the *z*-axis. Type α groups are constrained to move only 0.2 Å out of the surface plane, much less than in the lower coverages. These groups are tilted towards a surface oxygen atom, giving an $(O–H)_{non\text{-}bonded}$ separation of 2.36 Å. Despite the local stability of these surface structures, their surface energies are higher than that of 50% coverage (see Table 4) and therefore will not form.

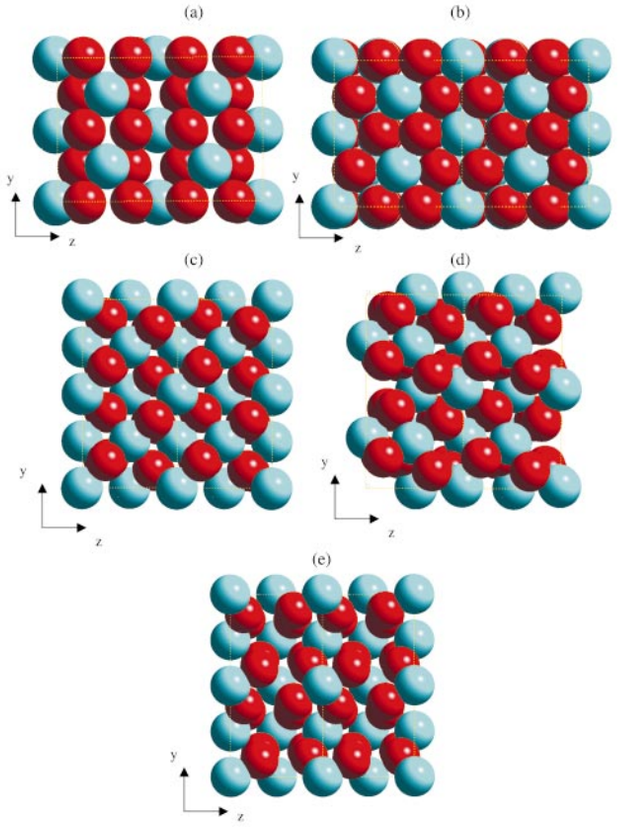

Fig. 4 Plan views of (a) (100) surface, (b) (101) surface, (c) (110)a surface, (d) (110)b surface and (e) (110)c surface (all under vacuum conditions).

3.2 The (101) surface

3.2.1 Dry (101) surface. The (101) surface has the lowest surface energy and is therefore the most stable face of tetragonal ZrO_2 under vacuum conditions. It is a type II surface[37] *i.e.* the surface has a stacking sequence of charged planes, but the repeat unit consists of several planes which when considered together have no dipole moment perpendicular to the surface. In this case, the repeat of the surface unit cell is formed from layers of O–O–Zr, and the surface is cleaved between the two oxygen layers. Surface relaxation is contained in the two uppermost layers, the Zr and O ions moving only

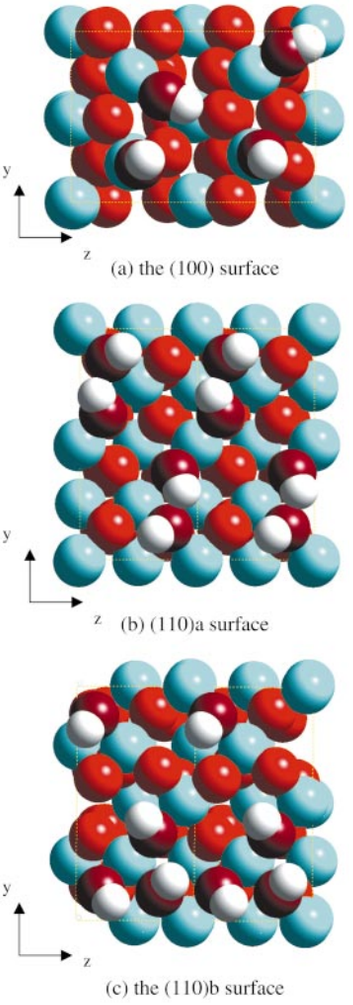

Fig. 5 Plan view of the 50% monolayer coverage of dissociated water on (a) the (100) surface, (b) the (110)a surface, (c) the (110)b surface.

0.08 and 0.05–0.15 Å towards the bulk crystal respectively. In the underlying layers, displacements are less than 0.05 Å. Surface cations and anions lose only one ligand each on the creation of this surface, with Zr ions in the surface layer 7-fold co-ordinate (similar to co-ordinations seen in zirconate pyrochlores and therefore quite stable),[39] and the O ions in 3-fold co-ordination. The relaxed structure is illustrated in Fig. 4(b).

3.2.2 25% Coverage. The presence of the water layer leads to only a very slight relaxation of the Zr cations, none being displaced more than 0.1 Å from their positions in the relaxed dry surface. In contrast, the oxygen ions move to a significant extent, with displacements of up to 0.3 Å in the layers within 4 Å of the surface plane, although beyond this relaxations are less than 0.1 Å. Nevertheless, the presence of surface hydroxide species has distorted this previously very stable surface.

All (OH) groups are oriented with the hydrogen atom pointing away from the crystal, leading to minimal interactions between them at this coverage. Type β groups are essentially in the pre-minimisation positions, with an O–H distance of 0.90 Å while type α groups have moved to be approximately 0.4 Å above the relaxed surface plane and have a longer O–H bond length of 0.96 Å.

The dry (101) surface is very stable with Zr, at least, highly coordinated. Thus it is not surprising that hydroxylation does not lead to further stability. Indeed, the hydroxylation energy is actually positive indicating that no hydroxylation will occur at this coverage. An equivalent observation was made by de Leeuw *et al.*[40] for the highly coordinated (100) surface of MgO.

3.2.3 All other coverages. At higher coverages, the hydroxylation energies continue to be positive. Therefore none of the coverages studied on the (101) surface results in an increase in stability.

Relaxations for higher coverages (50–100%) are similar to those described for 25% in that they lead to distortions of the underlying crystal, with the degree of distortion being found to increase with percentage coverage.

3.3 The (110) surface

The (110) is a type III surface,[37] *i.e.* alternately charged planes are stacked and produce a dipole moment perpendicular to the surface if cut between any plane of atoms. To stabilise the surface and remove the dipole, defects must be created (vacancies) in the surface layer. In fact, half of the surface ions must be removed. The stacking sequence of the surface unit cell of the (110) face is layers of O–Zr–O–Zr. Therefore, there are two terminations of this face, one at the oxygen plane and one at the Zr plane. If the surface repeat unit is formed from a single unit cell, this leads to 2 possible arrangements of the remaining O atoms (designated (A) and (B)) and one configuration of the Zr termination. All three possibilities have been investigated. Under vacuum conditions, termination (A) and (B) are almost equal in energy and more stable than the cation termination (designated (C)). Very similar conclusions were reached for the (200) surface of cubic CeO_2[41] and UO_2[42] – the (200) surface in the cubic system being the equivalent of the (110) in the present tetragonal system.

In the following sections, the hydroxylation of each termination is discussed separately.

3.3.1 Dry (110)A surface. The relaxation of the (110)A surface is much greater than that of the (100) and (101) faces. The oxygen atoms in the surface layer (which is only half occupied) are translated 1.1 Å from their bulk positions, away from the bulk crystal. This type of displacement also occurs in the underlying layers (which are fully occupied), but not all of the oxygen ions move to the same extent. Instead, those oxygen ions below the surface layer and beneath oxygen ions move less than those below a surface vacancy. Thus, each layer is split, leading to a new, ordered puckered structure. The magnitude of changes in oxygen ion positions decreases with depth but displacements of 0.1 Å are found up to 12 Å from the surface. The layers of Zr ions also pucker and relax to a greater extent than seen previously (up to 0.8 Å in the first Zr layer), with this translation being almost entirely perpendicular to the surface, away from the bulk crystal. Again, these displacements decrease with distance from the surface becoming less than 0.05 Å by a depth of 15 Å.

After relaxation, the surface layer consists of rows of alternating Zr and O atoms, running at 45° to both the *y* or *z* axes (Fig. 4(c)). The O atoms are 0.5 Å higher than the Zr atoms and are all at the same height, whereas the Zr atoms are at two different heights, separated by 0.4 Å.

3.3.2 25% Coverage. As the surface is hydroxylated, some of the vacant surface oxygen sites (created to remove the dipole of the type III surface) become occupied by (OH) groups. At 25% coverage a quarter of the vacant sites become occupied. Despite the additional occupancy of surface sites, the relaxation of the ZrO_2 crystal extends as far as under vacuum conditions and the magnitudes of the displacements are comparable to the pure surface. However, the surface hydroxide groups alter the symmetry of the puckered oxygen layers and lead to a lower symmetry relaxed structure in the bulk. The surface symmetry is also more complex. Now, the oxygen atoms relax closer to the cations, leading to the creation of small channels running along the *z* direction. The hydroxy groups are in pairs (consisting of 1 type α and 1 type β group) both tilted towards the surface at an angle of approximately 60°, with type α groups 1 Å above the surface and type β 2 Å. Their O–H bond lengths are somewhat different; 0.97 Å for type α and 0.91 Å for type β. Interactions between type α and β in a pair lead to a $(O–H)_{non\text{-}bonded}$ separation of just 1.62 Å, 0.1 Å shorter than found in ice.

3.3.3 50% Coverage. The relaxation of this crystal surface is very similar to that at 25% coverage and extends a similar distance into the crystal, although in general displacements are smaller. The hydroxy groups are again in equivalent pairs, but are now arranged differently. The specific arrangement is shown in Fig. 5(b): there are two pairs in each unit cell, related by a 180° rotation about the centre of the unit cell. The two types of (OH) group (α and β) are now at more similar distances from the surface plane, with a difference in height of only 0.3 Å. Their O–H bond lengths are also closer (type α 0.98 Å and type β 0.96 Å) indicating that the (OH) bond length again depends on distance from the surface. Within each pair, the $(O–H)_{non\text{-}bonded}$ separation is 1.77 Å. The hydroxylation energy at 50% coverage is small at just −0.32 eV per water molecule, but nevertheless leads to the largest reduction in surface energy of this face, consequently this is the maximum coverage predicted to occur.

3.3.4 75% and 100% coverage. At 75% coverage, all hydroxy groups interact with their neighbour *via* the oxygen and hydrogen atoms, leading to $(OH)_{non\text{-}bonded}$ separations between 1.9 and 2.5 Å. The relaxation of the ZrO_2 crystal is very similar in terms of both the sizes of the displacements and depth from the surface to that at 50% coverage.

A full monolayer leads to all hydroxy groups being equivalent. The hydroxy groups fill all vacancies formed by the removal of the dipole perpendicular to the surface. The surface is very smooth and the relaxation of the crystal is greatly reduced compared to that of the dry surface.

3.3.5 Dry (110)B surface. The surface relaxation of the (110)B surface (Fig. 4(d)) extends 12 Å into the crystal, but is

not as extensive as the relaxation of the (110)A surface. Again the lower oxygen layers are puckered, but the distortion is not so great as in termination (A) with a maximum displacement of 0.7 Å compared with 1.1 Å. The surface oxygen atoms relax to form zig-zag rows along the *z* direction.

The layers of Zr atoms below the surface remain in single planes, and are also displaced to a lesser degree than those of the (110)A, being translated by no further than 0.2 Å from their equilibrium positions, whereas those in the alternative (110)A were found to be displaced by up to 0.8 Å.

Although it is tempting to assume smaller relaxations imply an inherently more stable surface, this calculation shows that this is not necessarily true since the dry (110)B relaxed surface energy is effectively the same as that of the (110)A.

3.3.6 25% Coverage. At this low coverage, the (OH) groups on the (110)B surface are evenly spread. Type β groups tilt towards the surface at an angle of approximately 65°, and type α groups interact with a surface oxygen, resulting in an $(O–H)_{non\text{-}bonded}$ separation of 2.1 Å, the (OH) group making an angle of 30° with the surface. Type α groups have a marginally longer internal bond length than type β, 0.98 Å compared to 0.95 Å.

This low coverage leads to a breaking of the relaxed symmetry of the lower oxygen and zirconium layers, creating a structure similar to that of the (110)A face under vacuum conditions (section 3.3.1), except that in this case the ionic displacements are not as large, with maximum translations of 0.4 and 0.9 Å for Zr and O respectively. Ion displacements are less than 0.05 Å by a depth of 12 Å.

The energy (see Table 4) of the (110)B surface at this (and the 50%) coverage (see below) is somewhat lower than the corresponding (110)A surface. Thus, it seems that hydroxylation can change the way in which oxygen ions are arranged on dipolar surfaces.

3.3.6 50% Coverage. Relaxation of the ZrO_2 crystal is reduced at this coverage compared to the 25% coverage. In the uppermost Zr layer, displacements are between 0.3 and 0.5 Å, but by a depth of 8 Å, this has reduced to less than 0.1 Å. Similarly, the oxygen ions in the first two layers experience displacements between 0.3 and 0.9 Å, but 9 Å into the crystal, the ions displacements are less than 0.05 Å. The water layer is ordered, with rows of hydroxy groups running along the *y*-direction, spaced by 5.1 Å. Both types of group are tilted towards the surface, interacting with a neighbour to give a $(O–H)_{non\text{-}bonded}$ interaction with a separation of 1.6 Å. The hydroxy groups are at a similar height above the surface (types α and β are 1 and 1.3 Å above the surface respectively), leading to corresponding internal bond lengths of 1.01 and 0.96 Å. As in the case of (110)A, 50% monolayer coverage is the maximum coverage predicted for (110)B, although the resulting structures are quite different. The relaxed surface structures are illustrated in Figs. 5(b) and 5(c) for (110)A and (110)B respectively.

3.3.7 75% and 100% coverage. At 75% coverage, the hydroxy groups are arranged in two types of pair, one with an $(O–H)_{non\text{-}bonded}$ separation of 1.3 Å and one of 1.7 Å. These pairs are arranged in rows along the *z*-direction. Relaxation of the ZrO_2 crystal includes Zr ions in the uppermost layer being translated by up to 0.2 Å. Beyond this, cations exhibit changes in position of less than 0.05 Å. Displacements of oxygen ions at the surface are between 0.3 and 1.1 Å, but by a depth of 8 Å, and the ions in underlying layers relax to be less than 0.05 Å from their initial positions.

The structure of a complete monolayer formed on the (110)B surface is exactly the same as the (110)A, discussed in section 3.3.5.

3.3.8 Dry (110)C surface. The relaxation of the higher energy cation termination again involves the formation of puckered layers of both Zr and O atoms, reaching 12 Å into the crystal. The uppermost Zr atoms move away from the bulk crystal by up to 0.9 Å. The underlying oxygen layer moves in the same direction but a greater distance, becoming practically in plane with the zirconium layer. The structure of the resulting surface layer is quite open, exposing ions in the underlying layer. This leads to a rough surface topography with surface cations co-ordinated to only 4 oxygen atoms, two in the same plane and two below (Fig. 4(e)). Such a low coordination for the Zr^{4+} ion is inherently unstable and this surface exhibits a much higher surface energy that the (110)A and (110) B surfaces (see Table 4) and therefore is not predicted to form in dry conditions.

3.3.9 25% Coverage. The addition of the hydroxy groups to the cation termination of the (110) leads to a dramatic change in the relaxation of the crystal surface, with the creation of pyramid shaped facets, approximately 0.5 Å (2 atomic layers) in height, formed by a square of oxygen atoms topped with a cation. Each facet is then capped by a hydroxy group. Although the hydroxylation energy at this coverage is very large (−3.05 eV per water molecule), the surface energy of the hydroxylated (110)C is still much higher than the energies of the (110)A and (110)B structures and therefore will not form.

3.3.10 All other coverages. The facetted structure is seen at all coverages. As the partial coverage is increased, more of the surface oxygen atoms are protonated, leading to the formation of some triangular based facets. This continues up to full monolayer coverage, at which point each facet has two hydroxy groups associated with it. Although as mentioned previously, the hydroxylation energies are large and negative, the (110)C surface energies are high and therefore it is not predicted to occur under aqueous conditions.

4 Discussion and conclusions

The (O–H) potential model used in this work was fitted to a number of hydroxide crystal structures namely; NaOH, $Ca(OH)_2$, $Mg(OH)_2$, $Fe(OH)_2$, $Y(OH)_3$, FeOOH and AlOOH. The reason for this was to produce a potential model which allows for flexibility in (O–H) bond length, since in these compounds this distance ranges from 0.88 Å in $Fe(OH)_2$ to 1.13 Å in $Y(OH)_3$ *i.e.* the bond length is dependent on its environment. This work has shown that it is indeed necessary to allow for the occurrence of such deviations, since we have found that the surface environment also has a marked effect on the O–H bond length. In general, those further from the surface have shorter separations, while those closer to the surface are longer. The (OH) bond lengths found in this study were between 0.90 and 1.01 Å, which are within the range found in the compounds to which the potential was fitted.

At all partial coverages investigated on the (101) surface, the energies of hydroxylation were found to be positive. Therefore, we predict that this face will not hydroxylate. This is by far the most stable surface of tetragonal ZrO_2 under vacuum conditions, and thus might be expected to gain little stability from the formation of a chemically dissociated water layer (de Leeuw *et al.*[40] found a similar result for the most stable surface of MgO). Conversely, a hydroxide layer was found to stabilise the (100) and both oxygen terminations of the (110) surface, and consequently, the stabilisation of these faces in an aqueous environment with respect to the (101) is pronounced (see Table 3). However, for both surfaces the maximum degree of hydroxylation was provided by 50% monolayer coverage. This 50% coverage translates to an H_2O molecular surface density of 0.06 per $Å^2$ for the (100) surface and 0.03 $Å^2$ for the (110)

surface types. Similar densities are predicted to occur for the surfaces of MgO,[40] Fe_2O_3[43] and Mg_2SiO_4,[28] but in these systems, the percentage coverage required may be up to 100%.

Of particular interest was the effect that hydroxylation had on the (110) Type III surface. The distribution of oxygen vacancies on the (110) surface (which are necessary to remove the surface dipole[37]) was found to change depending on wet or dry conditions. In a dry environment, we find the (110)A and (110)B distributions to have effectively the same surface energies, but under aqueous conditions, the (110)B termination becomes clearly the most stable. In addition, the relaxation of the (110)B surface was different in the two environments, the hydroxy layer leading to a lower symmetry relaxed structure more reminiscent of the dry (110)A surface, although the displacements of ions from bulk positions are smaller in wet rather than dry conditions.

Under equilibrium conditions, the morphology of a single crystal is a result of the minimisation of the total surface free energy, and so is determined by the relative surface energies of the crystallographic faces[44] *i.e.* the surface with the lowest energy will make the highest contribution to the total surface area of the crystal. If we apply this to the results of our study, then under dry conditions, the (101) surface will dominate the crystal form, resulting in a modified octahedron. The (100) face does not contribute and the (110)A face contributes to a very minor degree. However, if placed in an aqueous environment, the relative surface energies of the (110)B surface decreases sufficiently with respect to that of the (101) that its contribution to the total surface area of the crystal will increase, changing the shape of the crystal. It is interesting to note that zirconia particles after heat treatment at 500 °C exhibit different morphologies depending on whether the treatment was in a wet or dry environment.[16] This behaviour is consistent with surface energies being moisture dependent.

It has been demonstrated that hydroxylation of a surface depends on crystallography. Thus, as the t→m surface transformation requires moisture, it follows that the propensity to transform may be a function of orientation. Furthermore, as the surface energies in the dry and wet states differ to an extent that depends on crystallographic face, the possibility exits that changes in surface tension could generate surface stresses in a polycrystalline sample that will affect the transformation. It has been suggested[16] that water may enhance the transformation by decreasing the difference between the surface energies of the tetragonal and monoclinic states. The present results, by demonstrating that water alters the surface energies of planes in the tetragonal structure, indicate that this hypothesis cannot be disregarded.

It should be borne in mind that the present modelling results are for pure zirconia whereas commercially available zirconia ceramics, and hence those for which the environment induced t→m has been investigated, contain stabilising oxides. Work is currently in progress to determine the effect of stabilising oxides on the surface energy and hydroxylation of the stabilised tetragonal phase.

Acknowledgements

Support for this work was provided by the EPSRC grant number GR/M 44903 *via* the ROPA scheme. Computing facilities were provided by the EPSRC grant number GR/M94427. R.W.G. gratefully acknowledges Los Alamos National Laboratory for support through the Bernd T. Matthias Scholarship.

References

1 R. H. J. Hannink, P. M. Kelley and B. C. Muddle, *J. Am. Ceram. Soc.*, 2000, **83**, 461.
2 N. Igawa, T. Nagasaki, Y. Ishii, K. Noda, H. Ohno, Y. Morii and J. A. Fernandez-Baca, *J. Mat. Sci.*, 1998, **33**, 4747.
3 T. Sato and M. Shimada, *J. Am. Ceram. Soc.*, 1984, **67**, C212.
4 A. H. Heuer, *J. Am. Ceram. Soc.*, 1987, **70**, 689.
5 M. Wilson, U. Schonberger and M. W. Finnis, *Phys. Rev. B; Condensed Matter*, 1996, **54**, 9147.
6 G. Jomard, T. Petit, A. Pasturel, L. Magaud, G. Kresse and J. Hafner, *Phys. Rev. B; Condensed Matter*, 1999, **59**, 4044.
7 J. K. Dewhurst and J. E. Lowther, *Phys. Rev. B; Condensed Matter*, 1998, **57**, 741.
8 M. W. Finnis, A. T. Paxton, M. Methfessel and M. van Schilfgaarde, *Phys. Rev. Lett.*, 1998, **81**, 5149.
9 F. L. Lowrie and R. D. Rawlings, *J. Eur. Ceram. Soc.*, 2000, **20**, 751.
10 M. V. Swain, *J. Mater. Sci. Lett.*, 1986, **5**, 1159.
11 B. Calles and Y. Stephani, *J. Mater. Sci. Med.*, 1994, **5**, 376.
12 J. J. Swabb, *J. Mater. Sci.*, 1991, **26**, 6706.
13 T. Sato, S. Ohtaki, T. Endo and M. Shimada, *High Tech.Ceramics* , ed. P. Vincenzini, Elsevier Science Publishers, B. V. Amsterdam, 1987, p. 281.
14 J. F. Li and R. Watanabe, *J. Am. Ceram. Soc.*, 1998, **81**, 2687.
15 X. Guo, *Solid State Ionics*, 1998, **112**, 113.
16 Y. Murase and E. Kato, *J. Am. Ceram. Soc.*, 1983, **66**, 196.
17 K. Grant and R. D. Rawlings, *J. Mater. Sci. Lett.*, 1999, **18**, 739.
18 K. L. Grant, R. D. Rawlings and R. Sweeney, submitted to *J. Mater. Sci: Mater. Med.*
19 J. Chevalier, B. Calles and J. M. Drouin, *J. Am. Ceram. Soc.*, 1999, **82**, 2150.
20 T. Sato and M. Shimada, *J. Am. Ceram. Soc.*, 1985, **68**, 356.
21 F. F. Lange, G. L. Dunlop and B. I. Davis, *J. Am. Ceram. Soc.*, 1986, **69**, 237.
22 M. Born and K. Huang, *Dynamical Theory of Crystal Lattices* , Oxford University Press, Oxford, 1954.
23 D. E. Parry, *Surf. Sci.*, 1975, **49**, 433.
24 D. E. Parry, *Surf. Sci.*, 1976, **54**, 195.
25 P. P. Ewald, *Ann. Phys.*, 1921, **64**, 253.
26 B. G. Dick and A. W. Overhauser, *Phys. Rev. B*, 1958, **112**, 90.
27 F. Jones, A. L. Rohl, J. b. Farrow and W. van Bronswijk, *Phys. Chem. Chem. Phys.*, 2000, **2**, 3209.
28 N. H. de Leeuw, S. C. Parker, C. R. A. Catlow and G. D. Price, *Phys. Chem. Miner.*, 2000, **27**, 332.
29 M. O. Zacate, L. Minervini, D. L. Bradfield, R. W. Grimes and K. E. Sickafus, *Solid State Ionics*, 2000, **128**, 243.
30 P. K. Schelling, S. R. Phillpot and D. Wolf, submitted to *J. Am. Ceram. Soc.*
31 D. H. Gay and A. L. Rohl, *J. Chem. Soc., Faraday Trans.*, 1995, **91**, 925.
32 D. D. Wagman, W. H. Evans, V. B. Parker, R. H. Schumm, S. M. Bailey, I. Halow, K. L. Churney and R. L. Nuttall, National Bureau of Standards Technical Notes, **270**(3–8).
33 J. D. Cox, D. D. Wagman and V. A. Medvedev, *CODATA Key Values for Thermodynamics*, Hemisphere Publishing, New York, 1989.
34 C. E. Moore, *Ionization Potentials and Ionization Limits Derived from the Analysis of Optical Spectra*, N. S. R. D. Ser., Natl. Bur. Stand. (U. S.), No. 341970.
35 K. P. Huber and G. Herzberg, *Molecular Spectra and Molecular Structure Constants of Diatomic Molecules*, Van Nostrand, New York, 1979.
36 L. M. Branscombe, in *Atomic and Molecular Processes*, ed. D. R. Bates, Academic Press, New York, 1962.
37 P. W. Tasker, *Philos. Mag. A*, 1979, **39**, 119.
38 B. Kamb, *Water and Aqueous Solutions*, ed. R. A. Horne, John Wiley & Sons Inc., New York, 1972.
39 L. Minervini, R. W. Grimes and K. E. Sickafus, *J. Am. Ceram. Soc.*, 2000, **83**, 1873.
40 N. H. de Leeuw, G. W. Watson and S. C. Parker, *J. Chem. Soc., Faraday Trans.*, 1996, **92**, 2081.
41 S. Vyas, R. W. Grimes, D. H. Gay and A. L. Rohl, *J. Chem. Soc., Faraday Trans.*, 1998, **94**, 427.
42 M. Abramowski, R. W Grimes and S. Owens, *J. Nuclear Mater.*, 1999, **275**, 12.
43 S. C. Parker, N. H. de Leeuw and S. E. Redfern, *Faraday Discuss.*, 1999, **114**, 381.
44 G. Wulff, *Z. Kristallogr.*, 1901, **34**, 449.